Nuclear Instruments and Methods in Physics Research A 749 (2014) 47–56

Contents lists available at ScienceDirect

Nuclear Instruments and Methods in Physics Research A

journal homepage: www.elsevier.com/locate/nima

Energy–angle correlation of neutrons and gamma-rays emitted from an HEU source

G. Miloshevsky *, A. Hassanein

Center for Materials under Extreme Environment, School of Nuclear Engineering, Purdue University, 400 Central Drive, West Lafayette, IN 47907-2017, USA

ARTICLE INFO

Article history:
Received 16 December 2013
Received in revised form
18 February 2014
Accepted 21 February 2014
Available online 2 March 2014

Keywords:
Special Nuclear Materials
Monte Carlo simulation
Energy spectra of neutrons and gamma-rays
Joint and marginal probability
density functions
Covariance and correlation

ABSTRACT

Special Nuclear Materials (SNM) yield very unique fission signatures, namely correlated neutrons and gamma-rays. A major challenge is not only to detect, but also to rapidly identify and recognize SNM with certainty. Accounting for particle multiplicity and correlations is one of standard ways to detect SNM. However, many parameter data such as joint distributions of energy, angle, lifetime, and multiplicity of neutrons and gamma-rays can lead to better recognition of SNM signatures in the background radiation noise. These joint distributions are not well understood. The Monte Carlo simulations of the transport of neutrons and gamma-rays produced from spontaneous and interrogation-induced fission of SNM are carried out using the developed MONSOL computer code. The energy spectra of neutrons and gamma-rays from a bare Highly Enriched Uranium (HEU) source are investigated. The energy spectrum of gamma-rays shows spectral lines by which HEU isotopes can be identified, while those of neutrons do not show any characteristic lines. The joint probability density function (JPDF) of the energy–angle association of neutrons and gamma-rays is constructed. Marginal probability density functions (MPDFs) of energy and angle are derived from JPDF. A probabilistic model is developed for the analysis of JPDF and MPDFs. This probabilistic model is used to evaluate mean values, standard deviations, covariance and correlation between the energy and angle of neutrons and gamma-rays emitted from the HEU source. For both neutrons and gamma-rays, it is found that the energy–angle variables are only weakly correlated.

1. Introduction

One of the critical gaps in homeland security is the inability to efficiently recognize samples of Special Nuclear Materials (SNM) [1]. These materials emit correlated neutrons and gamma-rays (gammas) with characteristic signatures [2]. The strategy for detecting the presence of SNM relies on sensing the emitted radiation [3,4]. In many modern neutron detectors, two features, multiplicity and time-correlation, are used as a way of distinguishing the different types of neutrons present in the flux [5]. Typical background consists of single neutrons and neutron groups from multiple neutron events caused by cosmic-rays [6]. To determine the presence of an SNM source, it is required to distinguish the SNM neutron count from random background or from correlated, but not SNM, sources such as those produced by cosmic-ray showers. Multiplicity analysis, neutron background correction methods, and cosmic-ray rejection algorithms are used in the neutron counters to eliminate a non-SNM source [5]. However, current detection systems do not have sufficient resolution to identify problematic amounts of fissionable material. The background radiation could be much more intense than the fission signature. The most challenging situation is the case where the count rate is near the background signal causing false alarms [4,7]. Responding to false alarms can be time consuming and expensive. The interaction of cosmic-rays with nearby metals can increase the background many times, making the detection of fission sources extremely difficult [8]. Most current detection systems rely on detecting "thermalized" neutrons [5]. Neutrons must be slowed down, which requires many centimeters of material surrounding the detector. Also, once the neutrons are slowed, their original energy and direction cannot be determined, rendering identification of SNM more difficult. The ability of SNM detectors to utilize other distributions such as the energy, angle, number, and lifetime of neutrons and gamma-rays can offer important improvements to recognize the presence of SNM.

To enhance detection of SNM, novel fast neutron counting technology was developed with high temporal and spatial resolution and capability to directly determine neutron energy and angle [9]. This technology, benefiting from advances in nanotechnology and organic semiconductors, combines the low-noise, high temporal and high spatial resolution of micro-channel plates (MCP) with the neutron-stopping power of hydrogen-rich plastic substrates. In MCP-based detectors, neutron detection is accomplished through the direct conversion of incoming fast neutrons into a pulse of electrons. The high timing resolution (~10 ns) of

* Corresponding author. Tel.: +1 765 494 8618; fax: +1 765 496 2233.
E-mail address: gennady@purdue.edu (G. Miloshevsky).

http://dx.doi.org/10.1016/j.nima.2014.02.042
0168-9002

the MCP-based device also allows efficient discrimination between neutrons generated in a fusion chain within SNM and background radiation. These novel technological advances stress the importance of understanding the joint probability distributions of various variables of neutrons and gammas emitted from an SNM source. Particle correlations in energy, angle, lifetime, and number (multiplicity) are many new parametric data that can be used to predict the intrinsic characteristics of the SNM source of neutrons and gammas. The joint and marginal probability density functions (JPDF and MPDF) of these parameters carry information about fission chains.

In this work, we have carried out Monte Carlo (MC) simulations of spontaneous fission chains in a low multiplying Highly Enriched Uranium (HEU) source using the developed MONSOL code. The spontaneous fission rate for 1 kg of HEU is only about ~3–4 neutrons per second that is less or comparable to those produced by cosmic-ray showers [10]. Therefore, it is very difficult to detect the HEU source using the passive detection methods. The MC simulations of an external source of neutrons interrogating HEU are also performed. Fission chains are induced by 60 keV neutrons. Our main goal in this research is to introduce the MONSOL code and identify the strength of relation between the energy and angle of neutrons and gamma-rays. From the MC simulations of spontaneous and interrogation-induced fission, the joint distributions of the energy and angle of neutrons and gamma-rays emitted from HEU sphere are created. A probabilistic model is developed to evaluate JPDF and MPDFs of energy and angle, mean values, standard deviations, covariance, and correlation. The paper is organized as follows: in Section 2 we describe the computational models; in Section 3 results and discussion are presented; conclusions are provided in Section 4.

2. Computational models

2.1. Fission chains in multiplying media

A characteristic feature of SNM sources is that they produce chains of fissions. After absorbing a neutron, the nucleus of ^{235}U becomes excited. Possible outcomes are the elastic scattering, fission, and nuclear reactions with the ejection of various particles. After fission or nuclear reactions, multiple (coincident) neutrons and gamma-rays are emitted, which in turn can induce subsequent fissions [10]. A chain of fissions and reactions with neutron emissions gives rise to a burst of neutrons and gamma-rays. The time scale for emission from fission chains is very short compared to that for neutron slowing down. Therefore, the burst of fission neutrons from a chain occurs almost instantaneous [11]. These bursts of particles can be detected and analyzed to infer the presence of SNM. The experimental studies of SNM sources require authorized access, time consuming planning, and scheduling of experiments. Therefore, validated simulation tools using faithful models are essential to characterize SNM fission signatures. The simulation capabilities are usually built upon high-quality fundamental nuclear cross-section and decay databases, allowing transport simulations to model the underlying physical phenomena accurately.

2.2. The MONSOL code

The MONSOL computer code is developed to perform MC simulations of the transport of neutrons and gamma-rays produced from the fission of SNM. A robust computational approach is implemented in MONSOL that covers the whole path from the fundamental nuclear reaction models and the inherent characteristics of the intra-nuclear and decay processes to the transport of neutrons and gamma-rays. The database of total and reaction cross-sections, energy spectra, angular distributions, and double-differential spectra of gammas and neutrons was created using the nuclear data tool TALYS [12]. This nuclear database is incorporated in the MONSOL code for MC simulations of fission chains in multiplying media. The following models are implemented: 1) database of nuclear-model parameters, RIPL-3, needed for nuclear data evaluations; 2) integrated coupled-channels optical model, ECIS06, for evaluation of total, elastic, reaction, and direct inelastic cross-sections, elastic and inelastic scattering angular distributions; 3) detailed structure of discrete levels for various fissionable isotopes; 4) pre-equilibrium particle emission based on a two-component exciton model; 5) equilibrium particle emission based on the Hauser–Feshbach model; and 6) various fission models including experimental, single- and double-humped fission, and the Wentzel–Kramers–Brillouin model.

The cross-sections of neutron interactions with ^{235}U nuclei calculated using MONSOL are shown in Fig. 1. The total cross-section is the sum of elastic, fission, and reaction cross-sections (Fig. 1(a)). A major contribution comes from the elastic scattering in the energy range from ~1 keV to ~200 MeV. The fission dominates over nuclear reactions, when the neutron energy is less than 0.5 MeV. At higher neutron energies, nuclear reactions are important,

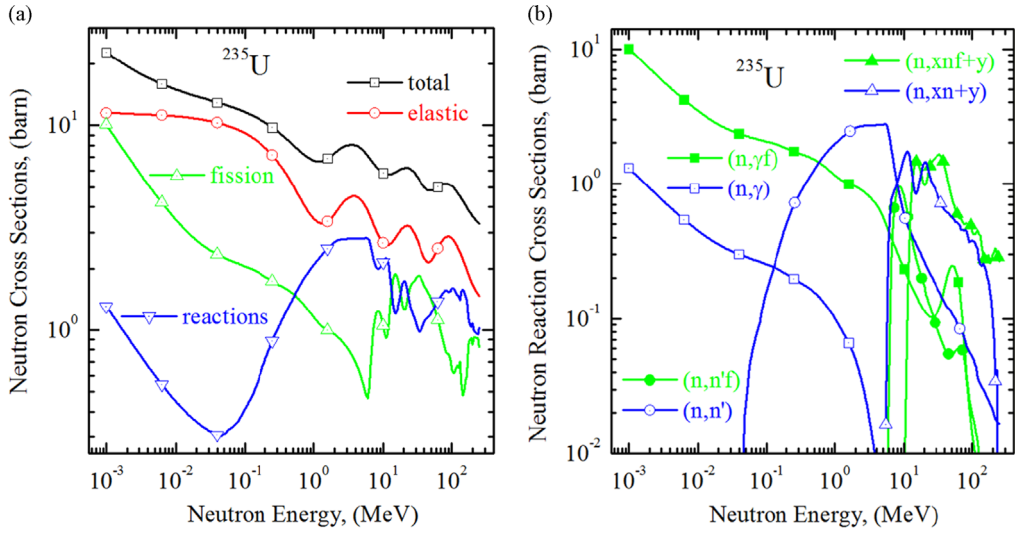

Fig. 1. Total, elastic, fission and reaction cross-sections of neutron interactions with ^{235}U nuclei (a) and decomposition of fission and nuclear reaction cross-sections (b).

especially in the range of energies from 1 MeV to 10 MeV. The type of reactions is decomposed in Fig. 1(b) for both fission and reaction channels. It is seen that the emission of gammas from fission and reactions dominates at low neutron energy. For reaction channel, the inelastic scattering of neutrons becomes important at $\sim >0.1$ MeV. The other particles can be emitted from excited ^{235}U nuclei at neutron energy $>\sim 7$ MeV. For fission channel, the inelastic scattering is observed in a narrow range of neutron energies, ~6–10 MeV. At higher neutron energy $\sim >10$ MeV, other particles are emitted from ^{235}U nuclei.

The detailed structure of the discrete energy levels of excited nuclei is implemented in MONSOL to describe accurately the radiative transitions. This is needed for accurate modeling of gamma decay of excited states of isotopes based on branching ratios and inelastic neutron scattering on discrete energy levels with later decay of an exited state by gamma emission. For instance, the energy of emitted gammas from heavy ^{235}U nuclei is within the range from ~45 keV to ~3 MeV. It is known that the density of energy levels decreases with decreasing the weight of nucleus. This means that the capture and inelastic scattering of neutrons on light nuclei can result in the emission of high-energy gammas (several MeV). This is important when the low-Z shielding materials are used.

To accurately describe the interaction of gammas with atomic electrons and nuclei, the NIST photon cross-sections [13] are implemented. The cross-sections of gamma interaction with ^{235}U are shown in Fig. 2. It is seen that at photon energies $\sim <0.1$ MeV, the photoelectric absorption on atomic shells and Rayleigh scattering are dominating processes. Compton scattering becomes important in the energy range between ~0.1 and 3.0 MeV, and the electron–positron pair production on ^{235}U nuclei dominates at higher energies. The photonuclear absorption of gammas is more than an order-of-magnitude lower compared to the electron–positron pair production. The photofission cross-section is even lower than that of photonuclear absorption.

The simulation of photon and neutron transport is straightforward because the mean number of interaction events in each MC history is fairly small. The flowchart of the MC method for modeling of neutron and photon trajectories [14] is described in Appendix A. Since the MONSOL code is a time-dependent MC code, it is possible to follow the time evolution of particles in a cascade. The algorithm works as follows. At the first interaction of a primary particle with matter the timing of cascade particles starts. The time interval that elapses as a particle moves along its path is computed by dividing the path step-length by an average particle's velocity (arithmetic mean of particle velocities in the beginning and in the end of step-length). Thus, the time is updated at interaction points. The total time elapsed since the first interaction is the sum of time intervals accumulated by successive particles. In this way, the MONSOL code is capable of calculating the lifetimes and arrival times of particles. The MONSOL code was recently used to study time correlations of cosmic-ray-induced background of neutrons and gamma-rays at sea level [15].

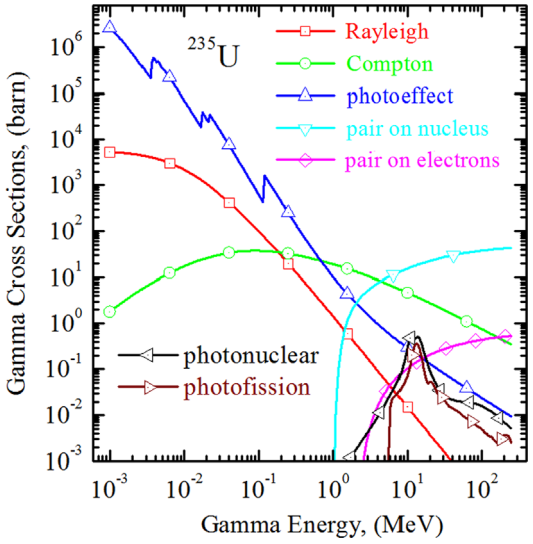

Fig. 2. Cross-sections of gamma interactions with ^{235}U nucleus.

2.3. Probabilistic model

The data obtained from MC simulations of SNM sources are used in a probabilistic model for analysis of the correlation of energy and angle of neutrons and gammas [16]. The JPDF of two variables x and y (for example, energy and angle of particles) to be observed together can be expressed as

$$p(x,y)\geq 0 \tag{1}$$

where $\int\int p(x,y)dxdy=1$. The MPDF is determined from Eq. (1) by integrating over one of variables, called "integrating out" that variable

$$p_X(x)=\int p(x,y)dy \text{ and } p_Y(y)=\int p(x,y)dx. \tag{2}$$

The variables are independent if their JPDF is the product of the MPDFs, i.e.

$$p(x,y)=p_X(x)\cdot p_Y(y). \tag{3}$$

The covariance is a measure of the strength of relation between variables

$$Cov(X,Y)=\iint (x-\mu_X)(y-\mu_Y)p(x,y)dxdy \tag{4}$$

where $\mu_X=\int x\cdot p_X(x)dx$ and $\mu_Y=\int y\cdot p_Y(y)dy$ are mean values. There could be either strong positive covariance, strong negative covariance, or covariance near zero. A positive covariance means that first variable is above (below) its mean value, when second variable is also above (below) its mean value. The correlation is the degree to which two or more variables are linearly associated

$$\rho_{X,Y}=\frac{Cov(X,Y)}{\sigma_X\cdot\sigma_Y} \tag{5}$$

where $\sigma_X=\sqrt{\int (x-\mu_X)^2p_X(x)dx}$ and $\sigma_Y=\sqrt{\int (y-\mu_Y)^2p_Y(y)dy}$ are the standard deviations. Positive correlation values indicate that the two variables are positively correlated, meaning that the two variables vary in the same direction. Negative values indicate that the two variables are negatively correlated, meaning that the two variables vary in the contrary direction. Values close to -1 or $+1$ reveal that two variables are highly related.

3. Results and discussion

3.1. Benchmarking the MONSOL code

For a widely varying set of nuclear reactions, the verification and validation of nuclear data used in MONSOL are well described in TALYS manual [17]. Total, elastic and inelastic cross-sections, photonuclear cross-sections, elastic and inelastic scattering angular distributions, fission cross-sections, recoil energy distributions, and reaction cross-sections of neutrons incident on different nuclei are compared to experimental data. An overall good agreement with experimental results is found confirming the reliability of TALYS nuclear data used in MONSOL. For further validation, the transport of neutrons and gammas should be benchmarked against the available data. The mean free path of neutrons in materials composed of light and heavy nuclei was compared to

experimental data [18]. The mean free path as a function of neutron energy calculated using MONSOL as an average over many free paths is shown in Fig. 3. It is seen that the calculated free paths of neutrons are in a good agreement with experimental data [18], especially for heavy elements and high neutron energies.

Using MONSOL, MCNPX [19] and GEANT4 [20] codes, MC simulations were carried out to investigate spontaneous and neutron-induced fissions in HEU sphere with a radius of 3.97 cm and mass density of 19.1 g/cm^3. The composition of U isotopes is 1.2% of ^{234}U, 93.3% of ^{235}U, and 5.5% of ^{238}U. The HEU has a very low rate of spontaneous fission, ~0.05 fissions/s in a sphere of radius 3.97 cm. Therefore, the count rate from HEU could be less or comparable to that from cosmic-ray-induced fission chains [10]. Cosmic-ray background may fluctuate making passive detection of HEU impossible. However, the rare fission chains can create a large number of neutrons and gamma-rays that can be detected [10]. Several snapshots of such long fission chains observed in MONSOL simulations of spontaneous fission in HEU are shown in Fig. 4. Bursts of neutron and gammas are seen at collision points due to nuclear reactions. Some of them are absorbed in HEU, and the others are escaped through the sphere's surface.

Fig. 5 compares the energy spectra of neutrons derived from MCNPX and GEANT4 codes to those produced by the MONSOL code. The energy spectra are normalized to the number of neutrons (an integral over the energy is unity) that escaped from the HEU sphere. For U isotopes, the energy spectrum of neutrons from spontaneous fission should be reminiscent of a typical Watt fission spectrum with a peak located near ~0.8 MeV [11]. There is a very good agreement between MONSOL and GEANT4 (Fig. 5(a)). However, the peak in the MCNPX spectrum is somewhat shifted toward the lower energies, ~0.4 MeV. This shift may indicate that the average number (multiplicity) of emitted neutrons in a spontaneous fission event is overestimated (larger than 1–2 neutrons for ^{235}U). All three energy spectra of neutrons do not show characteristic lines by which an isotopic composition can be identified. The energy spectra of neutrons escaped from a bare HEU sphere interrogated by 60 keV neutrons are shown in Fig. 5(b). The neutron spectrum from MONSOL and GEANT4 codes again compares very well. A large peak at ~60 keV corresponds to interrogating neutrons that reflected from the HEU sphere. However, the MCNPX energy spectrum shows a number of additional peaks in the low-energy region (Fig. 5(b)). These peaks are unphysical. The maximum of MCNPX fission energy is again shifted toward the lower energy (~0.4 MeV).

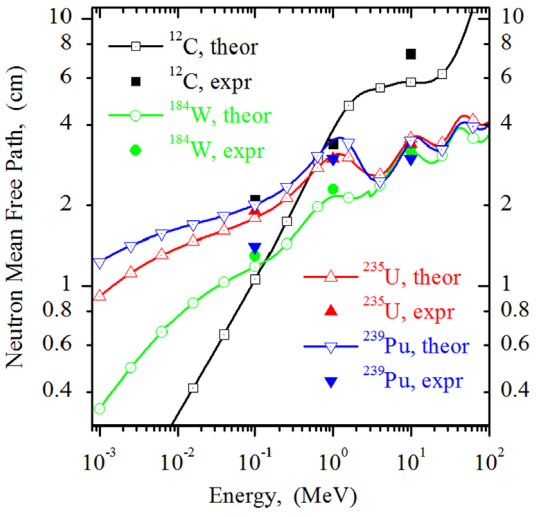

Fig. 3. Mean free path of neutrons in different materials as a function of energy.

For an interrogation-induced fission, the energy spectra of gammas from three codes show the characteristic lines in the keV region that differ in number and location (Fig. 6). The spectral lines in the MCNPX spectrum are obscure. The MONSOL spectrum is richer in the number of lines, since the fine detailed structure of energy levels and transitions is implemented in MONSOL. The broad energy maximum of gammas at ~0.6 MeV is nearly the same from the three codes. However, the GEANT4 spectrum shows a strong line near ~7 MeV, the origin of which cannot be explained for the case of an unshielded HEU sphere. MCNPX and MONSOL do not show any spectral line at this energy. We can conclude that the work is yet needed to correct and improve the fission models implemented in these codes, values of fission rates used, and details of energy levels and transitions in the excited nuclei.

3.2. JPDF and MPDF of energy–polar angle distributions of neutrons and gammas

A developed probabilistic model is used to post-process the simulated distributions of energy and polar angle of neutrons and gamma-rays emitted from a bare HEU sphere. The JPDF and MPDFs are constructed and the mean values, standard deviations, covariance and correlation of energy and polar angle are determined. The energy of neutrons and gammas leaving the HEU sphere is within the range from ~1 keV up to ~15 MeV. The MPDF of angular distribution of neutrons and gammas emitted from the sphere due to spontaneous fission is found to be uniform using the cosine units of polar angle (the reciprocal solid angle). However, the MPDF of angular distribution expressed in units of reciprocal degrees becomes non-uniform. We choose to display the angular MPDFs in reciprocal degrees and the polar angle in degrees in the range from 0° to 180°.

The JPDF map of the energy–polar angle distribution of neutrons escaping from the HEU sphere due to spontaneous fission is shown in Fig. 7(a). The polar angle is counted from the *Z*-axis, which is directed outward from the sphere's surface

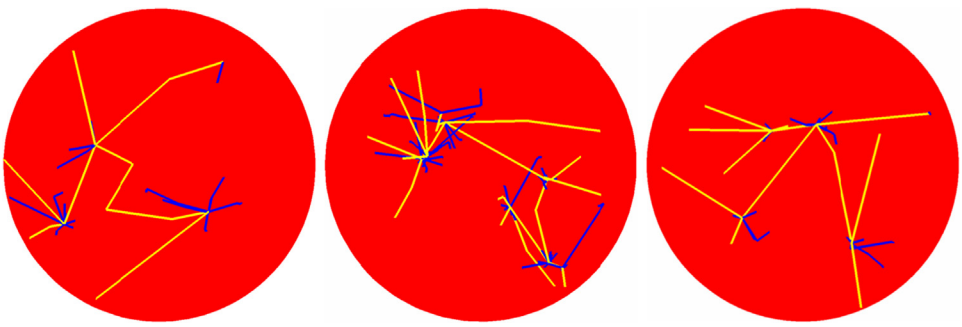

Fig. 4. Long fission chains in HEU generated in MONSOL simulation. Trajectories of neutrons and gamma-rays are in yellow and blue colors, respectively. (For interpretation of the references to color in this figure legend, the reader is referred to the online version of this article.)

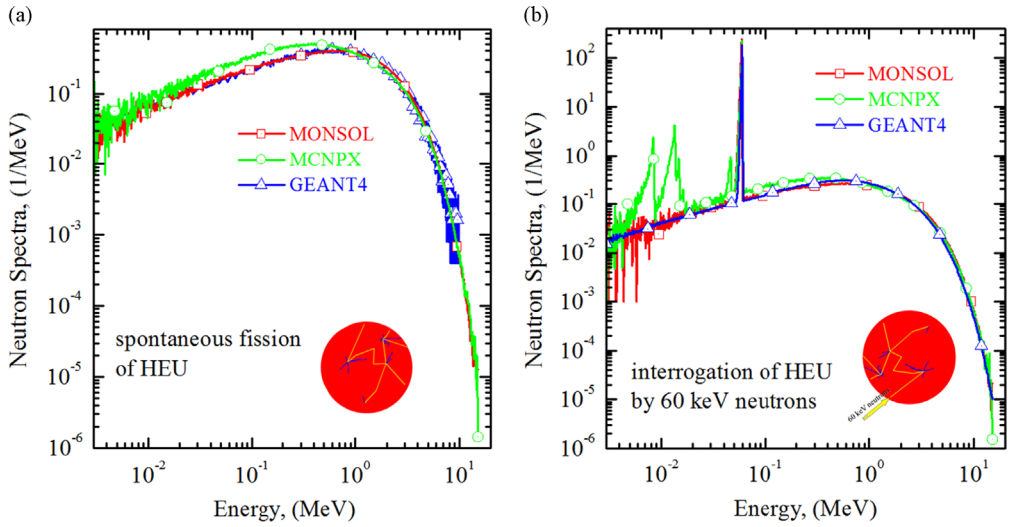

Fig. 5. Energy spectra of neutrons from (a) spontaneous and (b) interrogation-induced fission in an HEU sphere calculated using the MONSOL, MCNPX and GEANT4 codes.

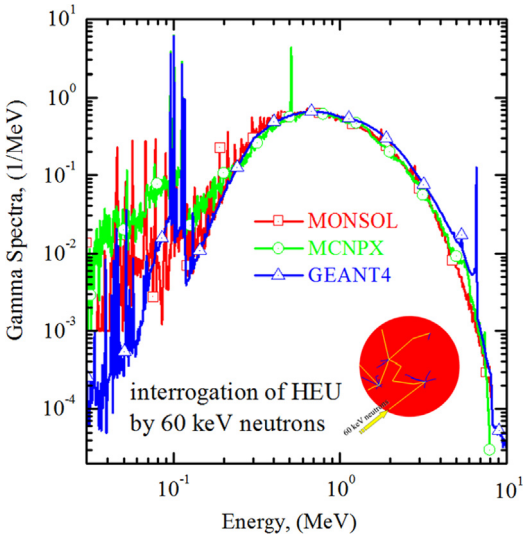

Fig. 6. Energy spectra of gammas from HEU sphere interrogated by 60 keV neutrons. The MONSOL, MCNPX and GEANT4 spectra are compared.

(inset in Fig. 7(b)). It is seen in Fig. 7(a) that neutrons are distributed within the whole angular range from 0° to 180° with a maximum near ~90°. The majority of neutrons is emitted with energies from ~0.1 MeV to ~2 MeV (Fig. 7(a)). The fraction of neutrons with lower energies <0.1 MeV and higher energies >2 MeV is considerably smaller. The MPDFs of energy and polar angle of neutrons can be derived by integrating over one of variables in Fig. 7(a). The MPDF of energy (actually the normalized energy spectrum) of neutrons leaving a bare HEU sphere is the same as that shown in Fig. 5(a). The peak of neutron energy is located at ~0.8 MeV. The MPDF of polar angle expressed in units of reciprocal degrees is illustrated in Fig. 7(b). The calculated mean values, standard deviations, covariance and correlation of neutron energy and polar angle in spontaneous fission are presented in Table 1. The covariance of neutron energy–polar angle relation, ~−0.019 MeV deg, is negative, meaning that both variables are below their mean values. The correlation, ~−0.00034, is also negative, meaning that energy and polar angle are varying in different directions. These variables are not strongly correlated, since their correlation value is negligibly small.

The JPDF of the energy–polar angle distribution of neutrons escaping from HEU sphere interrogated by 60 keV neutrons is shown in Fig. 8(a). In this case, the neutrons and gammas are generated in HEU due to the neutron-induced fission. It is seen in Fig. 8(a) that there is a strong line at 0.06 MeV across the entire range of polar angles. This line corresponds to the 60 keV neutrons reflected from an HEU sphere. The maximum of JPDF is located within ~0.1–2.0 MeV at ~90° corresponding to fission neutrons. Again as in the case of spontaneous fission (Fig. 7(a)), the fraction of neutrons with energies <~0.1 MeV and >~2 MeV is considerably reduced. The MPDFs of energy and polar angle of neutrons are derived by integrating over the energy and polar angle, respectively. The MPDF of energy represents the normalized energy spectrum of neutrons shown in Fig. 5(b) with a large peak at 0.06 MeV corresponding to the incident 60 keV neutrons reflected from the HEU sphere. The rest of the energy spectrum is a Watt fission spectrum with a maximum of fission energy nearly ~0.8 MeV. This portion of spectrum from neutron-induced fission compares well to the energy spectrum of spontaneous fission shown in Fig. 5(a). The MPDF of polar angle (Fig. 8(b)) is considerably modified compared to the case of spontaneous fission (Fig. 7(b)). The bell-shaped curve in Fig. 7(b) is transformed to the delta-peaked curve in Fig. 8(b). The height of peak at ~90° is increased about four times. This is due to a contribution of 60 keV neutrons. A schematic illustration is shown in the inset of Fig. 8(b). The incident 60 keV neutrons penetrate along the *X*-axis that makes 90° with the *Z*-axis. Therefore, the reflected neutrons mainly leave the HEU sphere at polar angle of ~90° in the direction of an interrogating beam. The statistic of correlations in this interrogation-induced fission is also modified (Table 1). The mean value of neutron energy, ~1.3 MeV, is lower compared to a case of spontaneous fission. However, the standard deviation, ~1.6 MeV, becomes higher. The mean value of neutron polar angle remains the same. Its standard deviation, ~32.3°, is lower. The covariance of neutron energy–polar angle, ~0.012 MeV deg, becomes positive. The correlation of neutron energy–polar angle, ~0.00024, also becomes positive but it remains very small.

Similar analysis is carried out for JPDF, MPDFs, mean values, standard deviations, covariance, and correlation of gammas emitted from the HEU sphere. The JPDF of the energy–polar angle distribution of gammas from spontaneous fission is shown in Fig. 9 (a). The gammas escape from HEU within polar angles 0–180°. It is seen in Fig. 9(a) that a maximum of the energy–angle distribution of gammas is located in the range corresponding to gamma energies ~0.4–1.0 MeV and polar angles ~60–120°. The fraction of lower- and higher-energy gammas is decreased within the

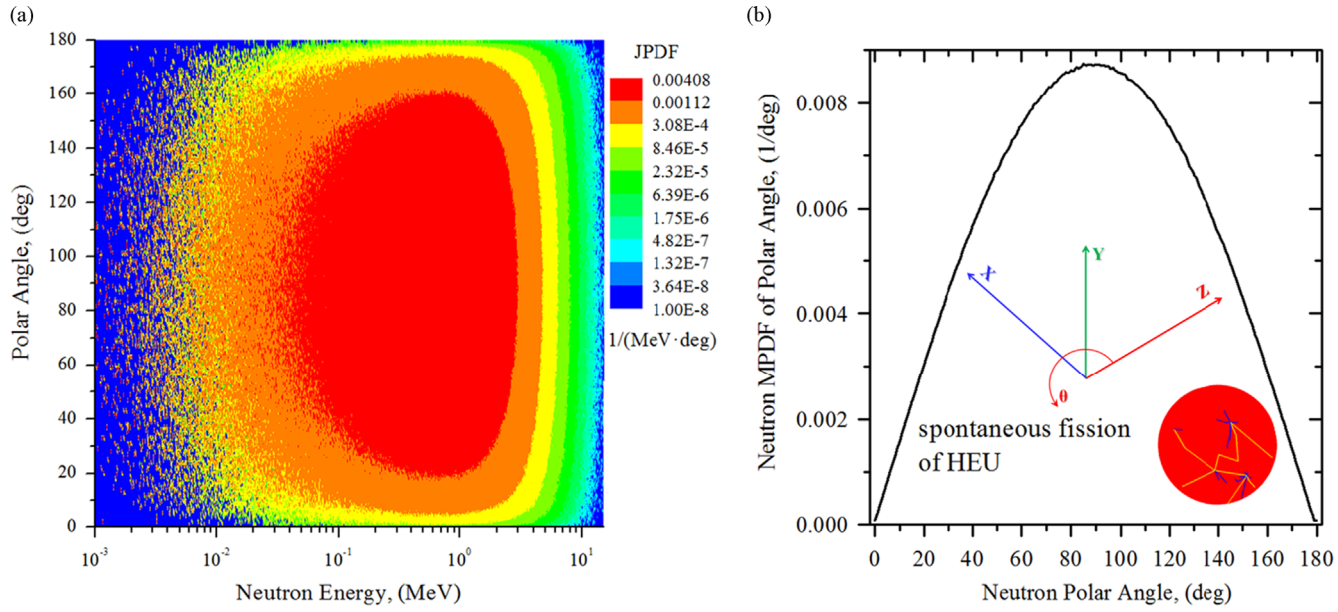

Fig. 7. JPDF of the energy–polar angle distribution (a) and MPDF of polar angle (b) of neutrons leaving a bare HEU sphere due to spontaneous fission.

Table 1
Mean values, standard deviations, covariance and correlation of energy and polar angle of neutrons emitted from a bare HEU sphere due to spontaneous and 60 keV neutron-induced fission.

	Energy (MeV)	Angle (deg)		Energy (MeV)	Angle (deg)
Spontaneous fission			**Interrogation-induced fission**		
Mean	~1.8	~89.5	**Mean**	~1.3	~89.5
Deviation	~1.4	~39.2	**Deviation**	~1.6	~32.3
	Energy–Angle			**Energy–Angle**	
Covariance (MeV deg)	~−0.019		**Covariance (MeV deg)**	~0.012	
Correlation	~−0.00034		**Correlation**	~0.00024	

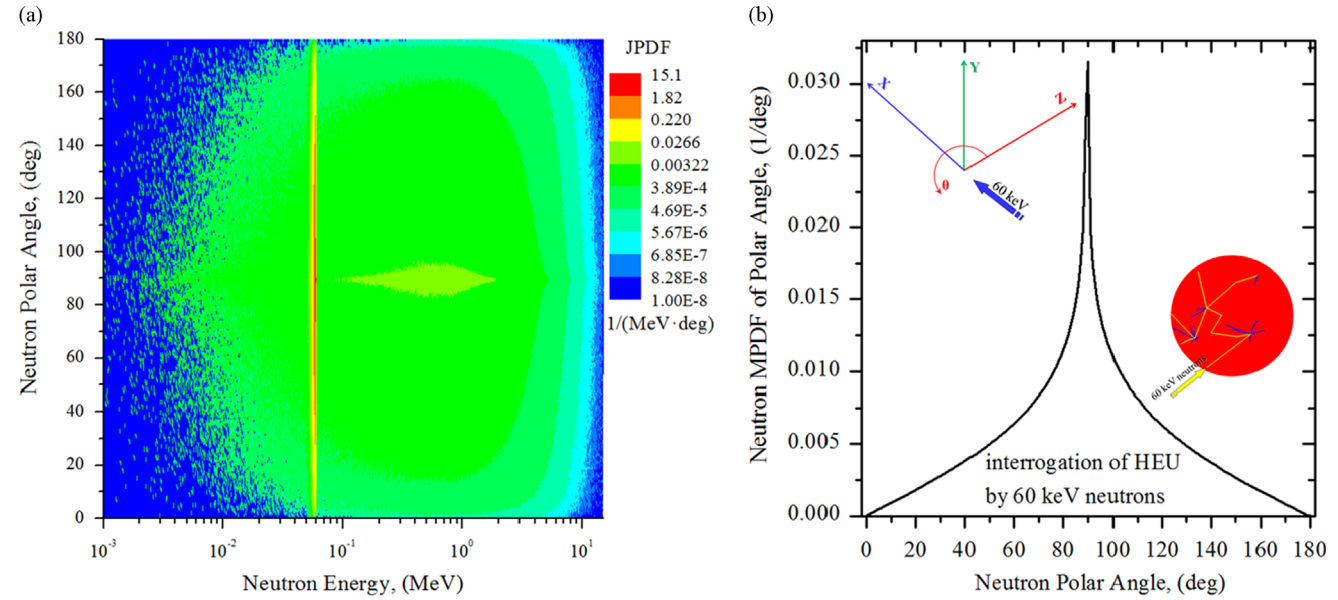

Fig. 8. JPDF of the energy–polar angle distribution (a) and MPDF of polar angle (b) of neutrons leaving a bare HEU sphere due to interrogation by 60 keV neutrons.

whole range of polar angles. There is a number of strips below ~0.3 MeV (Fig. 9(a)) corresponding to spectral lines. The MPDF of gamma energy is shown in Fig. 9(b). It is derived by integrating over polar angle in Fig. 9(a). The MPDF of gamma energy is the normalized energy spectrum of gammas from spontaneous fission. It shows a number of spectral lines in the keV region. The wide maximum of gamma energy is located at ~600 keV. The MPDF of polar angle of gammas in spontaneous fission is exactly the same as that of neutrons demonstrated in Fig. 7(b). In the discussion below, we therefore refer to Fig. 7(b) for MPDF of

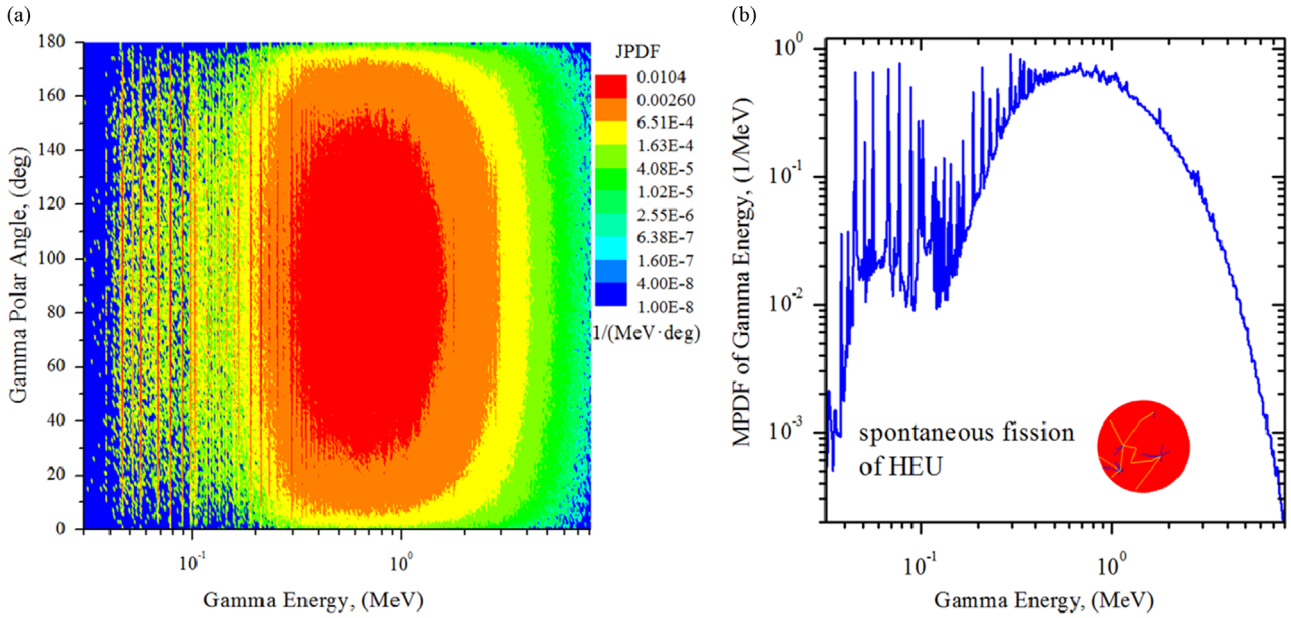

Fig. 9. JPDF of the energy–polar angle distribution (a) and MPDF of energy (b) of gammas escaping from a bare HEU sphere due to spontaneous fission.

Table 2
Mean values, standard deviations, covariance and correlation of energy and polar angle of gamma-rays emitted from a bare HEU sphere due to spontaneous and 60 keV neutron-induced fission.

	Energy (MeV)	Angle (deg)		Energy (MeV)	Angle (deg)
Spontaneous fission			**Interrogation-induced fission**		
Mean	~1.32	~89.5	**Mean**	~1.37	~89.5
Deviation	~0.92	~39.2	**Deviation**	~0.93	~28.6
	Energy–Angle			**Energy–Angle**	
Covariance (MeV deg)	~0.017		**Covariance (MeV deg)**	~0.0078	
Correlation	~0.00048		**Correlation**	~0.00029	

polar angle of gammas. When recalculated to the cosine units (the reciprocal solid angle), both gamma and neutron MPDFs of polar angle become uniform within a cosine range from −1 to 1. The mean values, standard deviations, covariance and correlation of energy and polar angle of gammas in spontaneous fission are presented in Table 2. The values of covariance and correlation of the energy–polar angle relation are small. It is seen that the energy and polar angle of gammas in spontaneous fission are very weakly associated.

The JPDF of the energy and polar angle distribution of gammas induced by 60 keV neutron interrogation in the HEU sphere is shown in Fig. 10(a). This JPDF is different compared to that corresponding to the case of spontaneous fission (Fig. 9(a)). There is a maximum of JPDF within the energy range from ~0.2 MeV to ~2 MeV near ~90°. The JPDF drops sharply for lower (< ~0.2 MeV) and higher (> ~2 MeV) gamma energies. The strips in the region below ~0.3 MeV are spectral lines. The MPDF of gamma energy (the normalized energy spectrum of gammas induced by 60 keV neutrons) is the same as that shown in Fig. 6. Both the spontaneous (Fig. 9(b)) and interrogation (Fig. 6) energy spectra of gammas are quite similar. The MPDF of polar angle of gammas emitted from the HEU sphere due to interrogation by 60 keV neutrons is illustrated in Fig. 10(b). The MPDF of gamma polar angle from interrogation (Fig. 10(b)) is different compared to that from spontaneous fission (Fig. 7(b)). The bell-shaped angular distribution of gammas is transformed to the strongly peak-shaped angular distribution. There is a large peak of gamma emission in the direction of the interrogating beam that is perpendicular to the *Z*-axis (inset in Fig. 10(b)). These gammas are produced due to the interaction processes of 60 keV neutrons with HEU nuclei. The height of polar angle peak (Fig. 10(b), interrogation case) increases about 6 times compared to that corresponding to the spontaneous fission (Fig. 7(b)). However, the statistics and correlations of gamma energy–polar angle are not considerably affected (Table 2). The mean value of gamma energy is ~1.37 MeV that is close to the case of spontaneous fission. The standard deviation of energy is nearly the same. Although the mean value of polar angle is the same, its standard deviation, ~28.6°, is lower. The covariance and correlation are small. Thus, it is found that the energy and polar angle of gammas from neutron-induced fission are very weakly correlated.

4. Conclusions

The MONSOL Monte Carlo code is developed by implementing comprehensive new optical nuclear models, various compound nuclei, fission, gamma-ray strength, level density, pre-equilibrium models, and nuclear structure parameters. The nuclear data tool TALYS was used to generate databases of cross-sections, energy spectra, angular distributions and double-differential spectra of gammas and neutrons. These nuclear datasets are incorporated in the MONSOL code for MC simulations of fission chains in multiplying media. For both cases of spontaneous and interrogation-induced fission, the energy spectra of neutrons and gammas from HEU sphere calculated using the MONSOL, MCNPX, and GEANT4

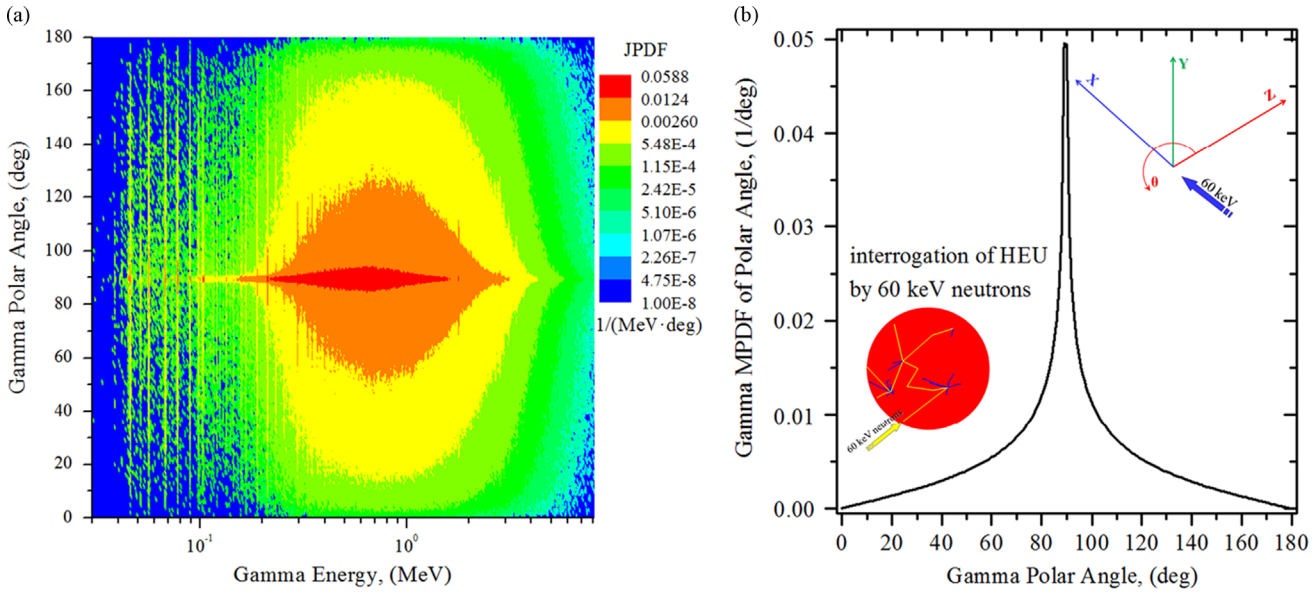

Fig. 10. JPDF of the energy–polar angle distribution (a) and MPDF of polar angle (b) of gammas induced by 60 keV neutrons in a bare HEU sphere.

codes are found in good agreement. The MONSOL code was then used to perform MC simulations of spontaneous and interrogation-induced fission chains in a low multiplying HEU. It is found that the energy spectrum of neutrons from spontaneous fission does not show characteristic lines by which HEU isotopes can be identified. The energy spectrum of neutrons from HEU interrogated by an external source of 60 keV neutrons shows a strong peak at ~60 keV corresponding to the interrogating neutron energy. The energy spectra of gammas from both spontaneous and interrogation-induced fission are found to be very similar. They demonstrate a series of spectral lines in the range from ~40 keV to ~400 keV which can be used to identify HEU isotopes.

From MC simulations, the joint distributions of energy and polar angle of neutrons and gammas are collected and analyzed. The calculated joint and marginal probability distributions are used in a developed probabilistic model for evaluation of the degree of association (correlation) between energy and polar angle of neutrons and gamma-rays emitted from HEU. The algorithms are implemented to calculate mean values, standard deviations, covariance and correlation. JPDFs and MPDFs of neutrons and gammas emitted from the HEU source are analyzed. The analysis is performed for spontaneous and neutron-induced fissions. For both neutrons and gammas, the angular MPDFs are found to be the same in spontaneous fission. This means that neutrons and gammas are uniformly emitted from the entire surface of the HEU sphere. The interrogation of HEU by 60 keV neutrons modifies the angular MPDFs of both neutrons and gammas. The emission of radiation becomes delta-peaked in the direction of the interrogating beam. This effect is more pronounced for gammas than neutrons. It is found that the energy and polar angle are only weakly correlated for both neutrons and gammas. The energy–polar angle correlation of neutrons (~ −0.00034) is of the same order of magnitude as that of gammas (~0.00048).

Acknowledgments

We thank Xue Yang, Nader Satvat, and Khaled Al-Shboul for calculating the energy spectra of neutrons and gamma-rays using the MCNPX and GEANT4 codes. This work is sponsored by the U.S. Department of Energy (DOE), National Nuclear Security Administration (NNSA), Office of Proliferation Detection (NA-221) under Grant no. DE-NA0000533.

Appendix A

According to the model of individual collisions, all elementary interactions of neutrons and gamma-rays with the medium are treated as individual events. The target is composed of 3D domains with constant material properties and interaction cross-sections. The 3D mesh is imposed in each domain. The flowchart for MC simulation of trajectories of neutrons and gamma-rays (noted as particles) implemented in the MONSOL code is shown in Fig. A1. The MC algorithm involves the following steps: 1) the initial energy ε, the angle of entrance $\vec{\Omega}(\alpha_x, \beta_y, \gamma_z)$ into Ith domain of the target, and the coordinates of entrance point $\vec{r}(x, y, z)$ of particle in cell (i,j,k) are sampled from particular distribution functions. Here α_x, β_y, and γ_z are direction cosines. 2) The optical free path-length is sampled as $l_{opt} = -\ln \xi$, where ξ is a random number. 3) The total macroscopic cross-section $\Sigma_{tot}^{I\text{th}} = \sum_{m=1}^{M} \Sigma_{tot}^{(m)}$ is calculated for Ith domain in which point $\vec{r}$ is located. Here $\Sigma_{tot}^{(m)}$ is the sum of macroscopic cross-sections of interaction processes of particle with mth component of atomic mixture in Ith domain. $\Sigma_{tot}^{(m)}$ is assumed to be a constant within Ith domain. For gamma-rays, the interaction processes are photoelectric absorption, Compton scattering, electron–positron pair production, Rayleigh scattering, and photonuclear reactions. For neutrons, the interaction processes are the elastic scattering, inelastic scattering, and various nuclear reactions. 4) The distance d to the boundary of Ith domain in direction $\vec{\Omega}$ is calculated. This distance is then expressed in terms of the optical thickness $d_{opt} = d \cdot \Sigma_{tot}^{I\text{th}}$. 5) If $l_{opt} > d_{opt}$ and a particle is located within the boundaries of target, then a new value of the optical free path-length is calculated as $l_{opt} = l_{opt} - d_{opt}$. In this case, a particle enters into a new I'th domain. The coordinates of entrance point $\vec{r}'$ in cell $(i', j',$ and $k')$ are calculated as $x' = x + d\alpha_x$, $y' = y + d\beta_y$, and $z' = z + d\gamma_z$. Further simulation of particle's trajectory is continued from step 3. 5) If $l_{opt} \le d_{opt}$, then the coordinates of collision point $\vec{r}'$ in Ith domain are calculated as $x' = x + L\alpha_x$, $y' = y + L\beta_y$, and $z' = z + L\gamma_z$, where $L = l_{opt}/\Sigma_{tot}^{I\text{th}}$. The indexes of cell $(i', j',$ and $k')$ in which point $\vec{r}'$

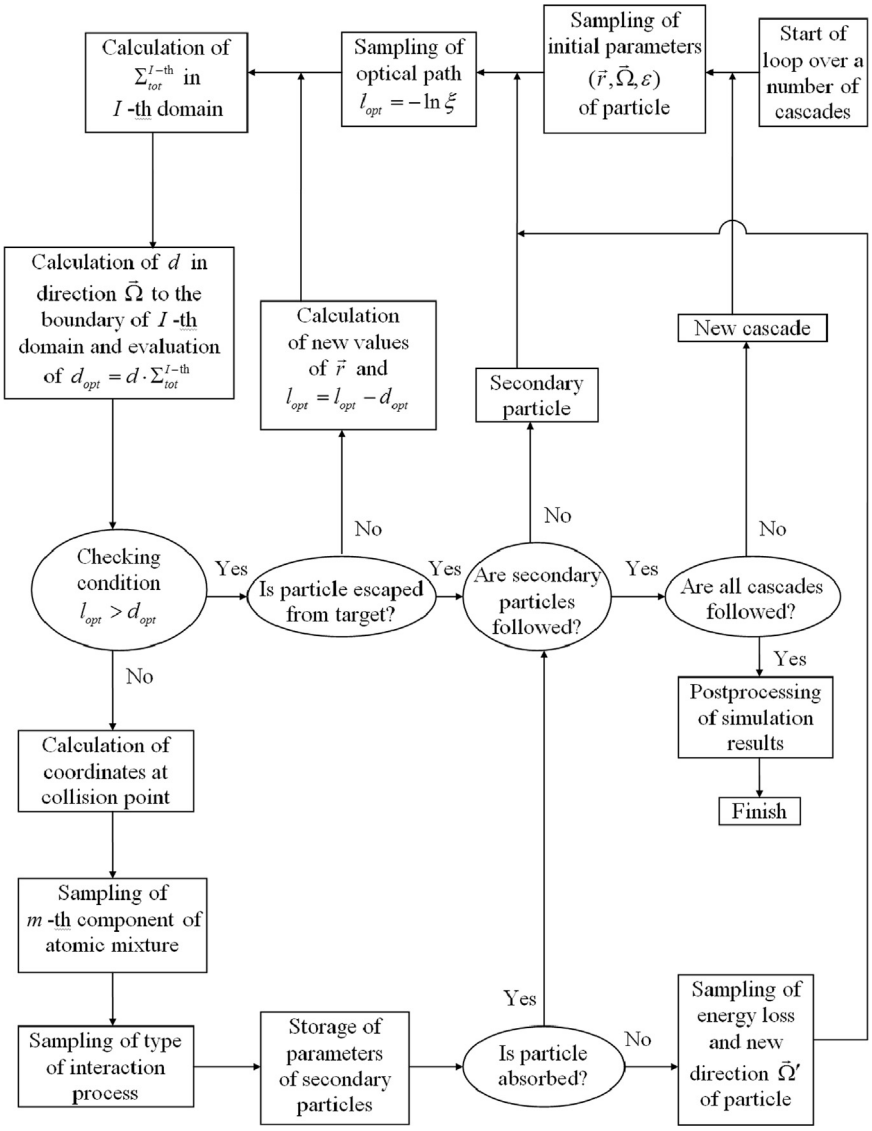

Fig. A1. Flowchart for Monte Carlo simulations of gamma-ray and neutron trajectories implemented in the MONSOL code.

is located are determined. 6) The mth component of atomic mixture with which a particle interacts is sampled as $\Sigma_{tot}^{(m)}/\Sigma_{tot}^{I\text{th}}$. 7) The type of the interaction process in cell (i', j', and k') is sampled as $\Sigma_n^{(m)}/\Sigma_{tot}^{(m)}$, where $\Sigma_n^{(m)}$ are macroscopic cross-sections of possible interaction processes of particle with mth component of mixture. In the case of absorption, particle's trajectory is terminated. Parameters of secondary particles are stored. 8) The transfer of energy $\Delta\varepsilon$ is sampled and it is deposited into cell (i', j', and k'). The new direction $\vec{\Omega}'$ of particle is calculated. Further simulation of particle's trajectory is continued from step 2. The above procedure is repeated until the particle's energy ε becomes lower than the cut-off energy or a particle is absorbed. The trajectory is also terminated when a particle crosses any boundary covering the target. Secondary particles are followed in a similar way.

References

[1] J. Medalia, Detection of nuclear weapons and materials: science, technologies, observations, Congressional Research Service, 2010 (CRS Report R401454 for Congress, Prepared for Members and Committees of Congress). Publisher: BiblioGov. Available at: 〈https://www.fas.org/sgp/crs/nuke/R40154.pdf〉.

[2] T. Gozani, IEEE Transaction on Nuclear Science NS-56 (2009) 736.

[3] G.W. Phillips, D.J. Nagel, T. Coffey, A Primer on the Detection of Nuclear and Radiological Weapons, Defense and Technology Paper 13, Center for Technology and National Security Policy, Washington, DC, 2005 (May).

[4] R.C. Runkle, D.L. Chichester, S.J. Thompson, Nuclear Instruments and Methods A 663 (2012) 75.

[5] N. Ensslin, W.C. Harker, M.S. Krick, D.G. Langner, M.M. Pickrell, J.E. Stewart, Application Guide to Neutron Multiplicity Counting, LA-13422-M Manual UC-700, 1998.

[6] P.K.F. Grieder, Cosmic Rays at Earth: Researcher's Reference Manual and Data Book, first ed., Elsevier Science Ltd., Amsterdam; New York, 2001.

[7] M. Owen, G. Weston, J. O'Malley, Proceedings of SPIE 7304 (2009) 73041K.

[8] R.T. Kouzes, J.H. Ely, A. Seifert, E.R. Siciliano, D.R. Weller, L.K. Windsor, M. L. Woodring, J. Borgardt, E. Buckley, E. Flumerfelt, A. Oliveri, M. Salvitti, Nuclear Instruments and Methods A 587 (2008) 89.

[9] D.R. Beaulieu, D. Gorelikov, H. Klotzsch, P. de Rouffignac, K. Saadatmand, K. Stenton, N. Sullivan, A.S. Tremsin, Novel fast neutron counting technology for efficient detection of special nuclear materials, in: 2009 IEEE Conference on Technologies for Homeland Security, 2009, pp. 287–293.

[10] J.M. Verbeke, A. Dougan, L.F. Nakae, K.E. Sale, N.J. Snyderman, Neutron correlations in special nuclear materials, experiments and simulations, in: Proceedings of 48th INMM Annual Meeting, Tucson, AZ, US, July 8–12, 2007.

[11] J.M. Verbeke, C. Hagmann, D. Wright, Simulation of Neutron and Gamma ray Emission from Fission and Photofission, Lawrence Livermore National Security, LLC, 2010 (UCRL-AR-228518). Available at: 〈http://nuclear.llnl.gov/simulation/fission.pdf〉.

[12] A.J. Koning, S. Hilaire, M.C. Duijvestijn, TALYS-1.0, in: O. Bersillon, F. Gunsing, E. Bauge, R. Jacqmin and S. Leray (Eds.), Proceedings of the International Conference on Nuclear Data for Science and Technology, ND 2007, April 22–27, 2007, Nice, France, EDP Sciences, 2008, pp. 211–214.

[13] ⟨http://www.nist.gov/pml/data/xcom/index.cfm⟩.
[14] G.V. Miloshevsky, Theoretical model on passage of particle fluxes of different types though inhomogeneous mediums and plasmas (Ph.D. thesis), The Institute of Heat and Mass Transfer of the National Academy of Sciences of Belarus, Minsk, Belarus, 1998, p. 183. Available at: ⟨https://engineering.purdue.edu/CMUXE/GenaPDFs/Thesis1998.pdf⟩.
[15] G. Miloshevsky, A. Hassanein, Nuclear Instruments and Methods A 737 (2014) 33.
[16] J.L. Devore, K.N. Berk, Modern Mathematical Statistics with Applications (Springer Texts in Statistics), 2nd ed., Springer, New York, 2012.
[17] ⟨http://www.talys.eu/documentation/⟩.
[18] S. Fetter, V.A. Frolov, M. Miller, R. Mozley, O.F. Prilutsky, S.N. Rodionov, R. Z. Sagdeev, Science Global Security. 1 (3–4) (1990) 225.
[19] MCNPX Version 2.5.0 User's Manual, LA-CP-05-0369, Los Alamos National Laboratory, 2005.
[20] S. Agostinelli, J. Allison, K. Amako, J. Apostolakis, H. Araujo, P. Arce, M. Asai, D. Axen, S. Banerjee, G. Barrand, et al., Nuclear Instruments and Methods A 506 (2003) 250.